Instant fabrication and selection of folded structures using drop impact

Supplementary material

Arnaud Antkowiak [*] , **Basile Audoly** [*] , **Christophe Josserand** [*] , **Sébastien Neukirch** [*] and **Marco Rivetti** [*]

[*]CNRS & UPMC Univ Paris 06, UMR 7190: Institut Jean Le Rond d'Alembert, 4 place Jussieu, F-75005 Paris, France

Submitted to Proceedings of the National Academy of Sciences of the United States of America

Experimental law for the fast initial spreading

We conducted a series of experiments with the aim to characterize the spreading Δ of an impacting drop on the same thin and narrow polymer strip as used in our '2D' experiments. Here, both the drop radius R and the impacting velocity U are varied. The results are reported in figure 1. The relative spreading $(\Delta - \Delta_0)/2R$ is plotted as a function of the Weber number $\mathrm{We} = \rho U^2 R/\gamma$. Here, Δ_0 represents the spreading in a quasi-static setting, when the drop is gently deposited on the flexible strip. The value of Δ_0 is extrapolated from the dataset and not measured directly; we find $\Delta_0 = 2.04$, 2.20, 1.96, 3.68 mm for $R = 1.2$, 1.5, 1.6, 1.85 mm respectively. The data for the different radii R all collapse on a single curve, indicating that the Weber number We is the relevant parameter for the spreading. A simple power law fits the data:

$$\frac{\Delta - \Delta_0}{2\,R} = 0.32\,\mathrm{We}^{1/2}, \qquad [1]$$

as shown in the figure.

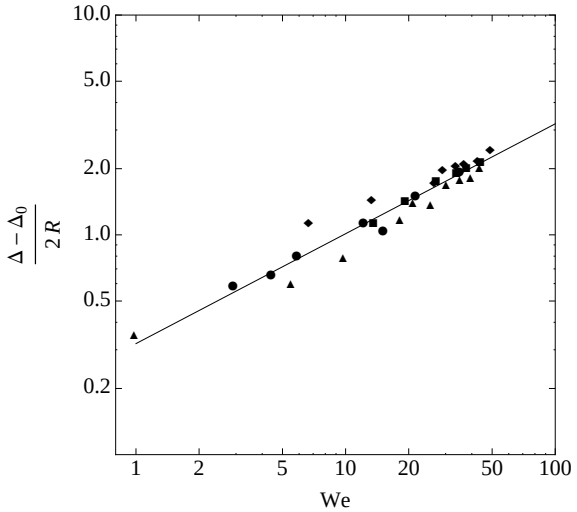

Figure 1. Spreading of a drop on a polymer strip. Different drop radii were used : $R = 1.2$ mm (▲), 1.5 mm (●), 1.6 mm (■) and 1.85 mm (♦). The dimensionless spreading length $(\Delta - \Delta_0)/2R$ is plotted as a function of the Weber number $\mathrm{We} = \rho U^2 R/\gamma$. The solid line is given by equation (1).

This experimental law is valid in our particular range of parameters. Its practical use is to allow confrontation of the experiments, where the velocity U is available, with the simulations, where the spreading length Δ is prescribed.

Calculation of fluid forces in the numerical code

Equations for dynamic, 2D Elastica. Let S be the arclength, t the time, and $\mathbf{x}(S,t)$ be the unknown position of centerline, see figure 2. The inextensibility condition writes $|\mathbf{x}'(S,t)| = 1$. Let then $\mathbf{t}(S,t)$ and $\mathbf{q}(S,t)$ be the unit tangent and normal to the centerline, respectively:

$$\mathbf{t}(S,t) = \mathbf{x}'(S,t), \qquad \mathbf{q}(S,t) = (-\mathbf{e}_y) \times \mathbf{t}(S,t). \qquad [2a]$$

Note that with these sign conventions, the local basis $(\mathbf{t}, \mathbf{q})$ is orthonormal and direct in the plane (x, z).

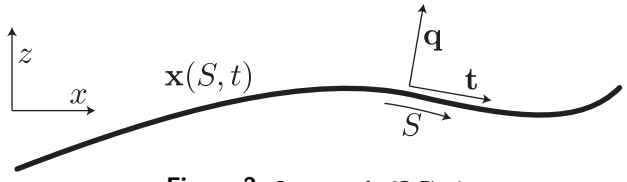

Figure 2. Geometry of a 2D Elastica

The signed curvature is defined by

$$\kappa(S,t) = \mathbf{x}''(S,t) \cdot \mathbf{q}(S,t). \qquad [2b]$$

We consider a linearly elastic, naturally straight strip with bending modulus $\hat{B}$. Its constitutive relation expresses proportionality between the curvature strain κ and the bending moment: $\mathbf{m}(S,t) = \hat{B}\,\kappa(S,t)\,(-\mathbf{e}_y)$. By the Kirchhoff equation for the balance of moment, $\mathbf{m}' + \mathbf{t} \times \mathbf{n} = 0$, the internal moment $\mathbf{m}$ has to be balanced by an internal force $\mathbf{n}$ of the form:

$$\mathbf{n}(S,t) = T(S,t)\,\mathbf{t}(S,t) - \hat{B}\,\kappa'(S,t)\,\mathbf{q}(S,t), \qquad [2c]$$

where the tension T is an unknown Lagrange multiplier associated with the inextensibility condition. The second Kirchhoff equation expresses the fundamental law of dynamics:

$$\hat{\mu}\,\ddot{\mathbf{x}}(S,t) = \mathbf{n}'(S,t) + \mathbf{p}(S,t). \qquad [2d]$$

Here, $\mathbf{p}(S,t)$ is the density of applied force, per unit length of the rod. Inserting equations (2a–2c) into equation (2d), we

Reserved for Publication Footnotes

obtain a nonlinear partial differential equation for the main unknown $\mathbf{x}(S,t)$ which is fourth order in space and second order in time. This is the classical equation for a dynamic Elastica in 2D. This equation of motion can be obtained by variational principles from the Lagrangian $\mathcal{L} = \mathcal{T} - \mathcal{U}$ given in main text, see for instance Ref. [1].

Quasi-static reconstruction of the drop. At every time, we determine the shape of the drop given the profile $\mathbf{x}(S)$ of the centerline — the time variable is omitted in the present Section. The shape of the drop is determined by the following requirements, see figure 3:

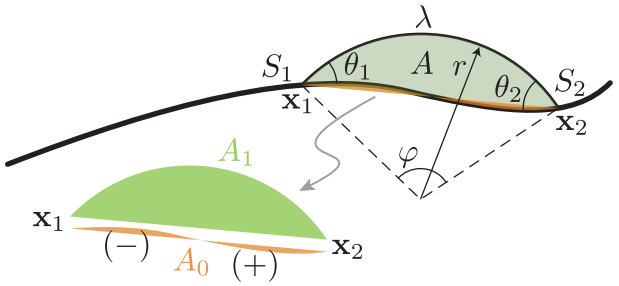

Figure 3. Quasi-static reconstruction of the fluid domain.

(i) the fluid-air interface is anchored to two points in space $\mathbf{x}_1 = \mathbf{x}(S_1)$ and $\mathbf{x}_2 = \mathbf{x}(S_2)$ that are prescribed, (ii) the length λ of this interface has to be minimal to make the capillary energy $(\hat{\gamma}\,\lambda)$ minimum, (iii) the area of the fluid, *i. e.* of the region enclosed by the fluid-air interface and by the wet part of the rod $\mathbf{x}(S)$ for $S_1 \leq S \leq S_2$, is constrained to a prescribed value A. The mass of fluid is neglected. This approximation suppresses capillary waves, and is consistent with the fact that the simulation resolves the elastic timescale τ_e, which is much larger than the capillary one, τ_c, see main text.

This constrained variational problem characterizes the equilibrium shape of a wetting fluid without gravity. Its solution is classical: the fluid-air interface is an arc of circle at equilibrium. The properties of this arc are determined as follows. First, we compute the signed area A_0 of the region enclosed between between the wet part of the rod, traced out by $\mathbf{x}(S)$ for $S_1 \leq S \leq S_2$, and the segment joining $\mathbf{x}_1$ and $\mathbf{x}_2$, with the sign conventions shown in figure 3. The area A_1 of the circular cap shown in green in the figure, enclosed between the fluid-air interface and the segment $[\mathbf{x}_1, \mathbf{x}_2]$, is $A_1 = A - A_0$. The angle φ of the circular cap is then calculated by solving the following geometric relation:

$$\frac{A_1}{|\mathbf{x}_1\mathbf{x}_2|^2} = \frac{\varphi - \sin\varphi}{8\,\sin^2\frac{\varphi}{2}}.$$

The radius r and the perimeter λ of the circular cap are then found by

$$r = \frac{|\mathbf{x}_1\mathbf{x}_2|}{2\,\sin\frac{\varphi}{2}}, \qquad \lambda = \varphi\, r.$$

Finally, the angles θ_1 and θ_2 of the fluid-air interface with respect to the local frame $(\mathbf{t}, \mathbf{q})$ are given by

$$\theta_1 = \frac{\varphi}{2} + \angle(\mathbf{t}_1, \mathbf{x}_2 - \mathbf{x}_1), \qquad \theta_2 = \frac{\varphi}{2} + \angle(\mathbf{x}_1 - \mathbf{x}_2, -\mathbf{t}_2),$$

where $\angle(\mathbf{a}, \mathbf{b})$ denotes the signed measure of the angle made by the vectors $\mathbf{a}$ and $\mathbf{b}$, and $\mathbf{t}_1 = \mathbf{x}'(S_1) = \mathbf{t}(S_1)$ and $\mathbf{t}_2 = \mathbf{x}'(S_2) = \mathbf{t}(S_2)$ denote the unit tangents at the two points of contact of the interface with the rod. Note that the angles θ_1 and θ_2 are different from the equilibrium value set by the Young-Dupré relation since the contact line is pinned.

In the simulation we do not implement any mechanism preventing the fluid-air interface from crossing the rod. A spurious crossing is visible in the inset labelled D′ in fig. 5b of main text. Overlooking the collisions of the fluid-air interface with the rod is justified *a posteriori* by the fact that we observed such collisions in only one instance, which is precisely the simulation labelled D − D′. Even then the crossing took place during a short time interval, just after the anchor point S_2 was moved to the right. In addition this crossing takes place over a region much smaller than the size of the drop. As a result, its impact on the simulation is very limited.

Expression of forces. We consider three types of forces, with total lineic density $\mathbf{p}(S,t)$:

$$\mathbf{p}(S,t) = \mathbf{p}_\mathrm{g}(S,t) + \mathbf{p}_\mathrm{c}(S,t) + \mathbf{p}_\gamma(S,t), \qquad [3]$$

where $\mathbf{p}_\mathrm{g}$ denotes the weight of the Elastica, $\mathbf{p}_\mathrm{c}$ the reaction of the support, and $\mathbf{p}_\gamma$ the capillary forces.

The weight is given in terms of the mass per unit length $\hat{\mu}$:

$$\mathbf{p}_\mathrm{g}(S,t) = -\hat{\mu}\,\mathbf{e}_z. \qquad [4]$$

In the absence of friction on the ground, the contact force reads:

$$\mathbf{p}_\mathrm{c}(S,t) = p_\mathrm{c}(S,t)\,\mathbf{e}_z \qquad [5]$$

where $p_\mathrm{c} \geq 0$ is the unknown contact pressure with the ground. This force is associated with the unilateral constraint $\mathbf{x}(S)\cdot\mathbf{e}_z \geq 0$. Note that $p_\mathrm{c} = 0$ when there is no contact, *i. e.* $\mathbf{x}(S)\cdot\mathbf{e}_z > 0$. In the implementation, we avoid calculating the contact pressure p_c as collision response is treated using an impulse-based model.

The capillary force is made up of two point-like forces, acting at the points of contact S_1 and S_2 and represented by Dirac distributions, and a distributed force arising from the capillary pressure inside the drop:

$$\mathbf{p}_\gamma(S,t) = \mathbf{f}_1\,\delta(S-S_1) + \mathbf{f}_2\,\delta(S-S_2) + \mathbf{f}_\mathrm{p}(S)\,H(S-S_1)\,H(S_2-S), \qquad [6]$$

where the Heaviside function H is used here to restrict the support of the last term to the wet region, $S_1 < S < S_2$. The point-like forces $\mathbf{f}_1$ and $\mathbf{f}_2$ are directed along the fluid-air interface, and represent line tension:

$$\mathbf{f}_1 = \hat{\gamma}\,(\mathbf{t}(S_1)\,\cos\theta_1 + \mathbf{q}(S_1)\,\sin\theta_1), \qquad [7a]$$
$$\mathbf{f}_2 = \hat{\gamma}\,(-\mathbf{t}(S_2)\,\cos\theta_2 + \mathbf{q}(S_2)\,\sin\theta_2). \qquad [7b]$$

The distributed force $\mathbf{f}_p$ is the pressure force arising from capillary pressure

$$\mathbf{f}_p(S) = -\frac{\hat{\gamma}}{r}\,\mathbf{q}(S). \qquad [8]$$

These capillary forces can be derived from the capillary energy $(\hat{\gamma}\,\lambda)$ by variational principles.

Selection of final shape in the absence of gravity

Here we show that the final pattern can be selected by the impact velocity even in the absence of gravity. Gravity was considered in the main text as it allows to set up well-controlled experiments showing quantitative agreement with the numerics.

Figure 5 shows time sequences for two numerical experiments with the same parameters, except for the spreading Δ. Figure (5a) makes use of a smaller spreading length

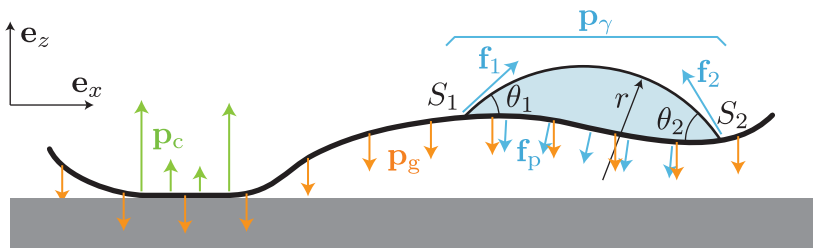

Figure 4. Forces applied on the elastic filament: capillary forces $\mathbf{p}_\gamma$, weight $\mathbf{p}_g$, and contact forces from the support $\mathbf{p}_c$.

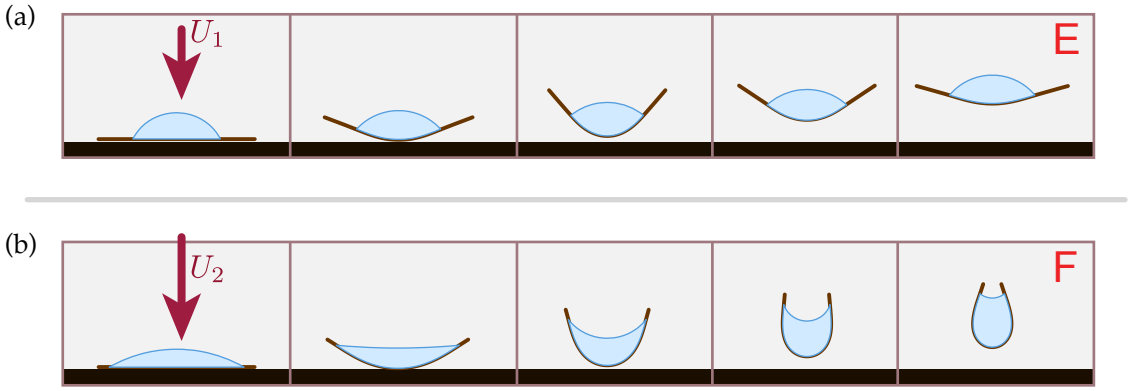

Figure 5. Time sequences illustrating selection in the absence of gravity: by increasing the spreading length without modifying the other parameters, the final state goes from (a) unencapsulated to (b) encapsulated. Parameters common to both simulations are rescaled drop area $A/{\ell_{ec}}^2 = 1.5$ and rod length $L/\ell_{ec} = 4.6$. A small damping is enforced using a viscous drag coefficient per unit length $\mathrm{d}b/\mathrm{d}s = 1.04\,(\hat{\mu}\,\hat{B})/\ell_{ec}^2$. Different drop impacts are simulated using (a) $\Delta/\ell_{ec} = 2.5$ for a slower impact and (b) $\Delta/\ell_{ec} = 4$ for a slower impact. Overall duration of the time sequences is $t = 8.4\,(\hat{\mu}/\hat{B})^{1/2}$. See also supplementary movie S4.

$\Delta = 2.5\,\ell_{ec}$, corresponding to a slower impact velocity, than in figure (5b), for which $\Delta = 4\,\ell_{ec}$. Encapsulation is observed with the larger spreading length only, leading to the same findings as in the experiments of Figure 2 in main text (dynamic impact on a flower-shaped target without long arms).

The possibility of a transition from unencapsulated to encapsulated final states can be understood by looking at the branches of equilibria for fixed rod length L, drop area A and elasto-capillary length ℓ_{ec}. These branches are plotted in figure 6 for the same parameters as used in the time sequences of figure 5. A bistability is observed for some values of spreading length Δ, as in reference [2]. For sufficiently large spreading width Δ, the kinetic energy of the impacting drop is converted into capillary energy (captured by the numerical parameter Δ) and back into kinetic energy, allowing the bundle to jump onto the encapsulated branch from an initially flat configuration.

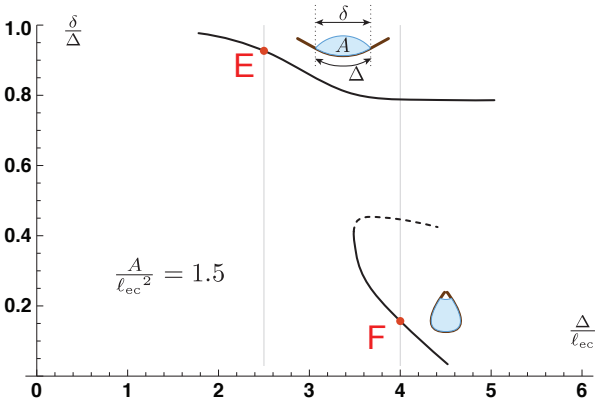

Figure 6. Equilibrium configurations in the absence of gravity, for $A/\ell_{ec}^2 = 1.5$ and $L/\ell_{ec} = 4.6$ (same parameters as in figure 5). The x axis is the rescaled length Δ of the fluid-solid interface, and the y axis measures encapsulation. For some values of the parameters, multiple equilibrium configurations are in competition.

1. B. Audoly and Y. Pomeau, Elasticity and geometry: from hair curls to the nonlinear response of shells (Oxford University Press, 2010).

2. Py C., Reverdy P., Doppler L., Bico J., Roman B., Baroud C. N. (2007) Capillary Origami: Spontaneous Wrapping of a Droplet with an Elastic Sheet. Phys. Rev. Lett. 98:156103